# Multi-Dimensional Upwind Schemes, Multigrid and Defect Correction for Accurate and Efficient Euler Flow Computations

B. Koren and P.W. Hemker
CWI
P.O. Box 4079, 1009 AB Amsterdam, The Netherlands

**Abstract**

Two multi-dimensional upwind discretizations for the steady Euler equations are presented, one with a good multigrid efficiency and the other with a good multi-dimensional accuracy. The two discretizations consist of a one-dimensional Riemann solver with locally rotated left and right cell face states. For non-hypersonic flow computations, a standard nonlinear multigrid iteration is applied. For hypersonic flow computations, a nonlinear multigrid technique with improved robustness is presented. The robustness improvements consist of a local damping of the restricted defect and a global upwind prolongation of the correction. For the steady, two-dimensional Euler equations, numerical results are presented first, for some supersonic test cases with an oblique contact discontinuity and an oblique shock wave. Next, results are shown for a hypersonic reentry flow around a blunt forebody with canopy.

*Key Words:* steady Euler equations, supersonic and hypersonic flows, multi-dimensional upwind schemes, multigrid iteration, defect correction iteration.
*Note:* This work was supported by the European Space Agency, through Avions Marcel Dassault - Bréguet Aviation.

## 1 Introduction

### 1.1 Grid-coupled 1-D upwind schemes

Many upwind schemes used in multi-dimensional (multi-D) flow computations are based on the application of some one-dimensional (1-D) shock capturing scheme in a grid-aligned manner. Despite the rigorous mathematics involved in these 1-D upwind schemes, in most multi-D flow computations, the underlying 1-D upwind results are just superposed without rigorous mathematical justification. Besides this inconsistency in methodology, the grid-alignment (i.e. grid-dependency) is also inconsistent with the upwind principle that discretizations should be dependent on the solution only. In practice, the above deficiencies are counterbalanced to a large extent by the advantage of simplicity in implementing the grid-aligned 1-D upwind approach. Further, for many practical purposes, very satisfactory multi-D results are obtained by applying the grid-aligned 1-D upwind approach.

However, sometimes the aforementioned flaws become clearly visible in the numerical results. For instance, the resolution of layers that are not aligned with the grid (and hence neither with the discretization) may be insufficient; oblique layers may be falsely diffused to an unacceptable extent. Simply lowering the magnitude of false diffusion by raising the order of accuracy of the underlying 1-D upwind scheme may help, but - possibly - at a very high increase in computational cost. A more proper balance is wanted between (multi-D) accuracy and efficiency. To achieve such a balance, one needs not just control false diffusion's magnitude, but - separately - both its magnitude and its direction. From a viewpoint of consistency, it seems most natural to no longer ignore the multi-D nature of a multi-D flow in the upwind scheme itself.

### 1.2 Grid-decoupled multi-D upwind schemes

Several grid-decoupled multi-D upwind discretizations have been published already and many more are still in development. Relevant methods in this field are: (i) the rotated flux methods as proposed by Davis (Ref. 2) and Levy et al. (Ref. 15), and (ii) the methods, proposed by Roe (Ref. 18) and Hirsch et al. (Ref. 8), which (try to) decompose the coupled system of Euler equations into a set of scalar convection equations. In Ref. 6, a brief survey is given of existing multi-D upwind approaches.

Despite the large amount of theoretical work which has been put already into the development of multi-D upwind schemes, so far it can be concluded that the quality of the numerical results is not yet quite satisfactory. Of course, much work on these schemes is still in progress.

### 1.3 Efficient solution methods

Though the emphasis in most multi-D upwind research clearly lies on a good accuracy, some work has also been directed already towards a good efficiency.

Examples in the context of explicit time stepping schemes are the work of LeVeque (Ref. 14) and the work of Catalano and Deconinck (Ref. 1). In Ref. 14 a technique is presented for improving the (multi-D) stability restriction on the time step. In Ref. 1, the aim is not just good stability, but also a good multi-D damping of high-frequency errors, the latter for the sake of a fruitful multigrid acceleration.

As far as we know, the only implicit solution methods for multi-D upwind discretizations are those proposed by Hirsch and Lacor (Ref. 9), and Sidilkover (Ref. 19). Whereas Hirsch and Lacor consider unsteady flow equations, Sidilkover considers steady flow equations, and solves these directly (i.e. not through any unsteady form) by means of a multigrid method. A direct multigrid solution approach applied to steady, multi-D upwind discretizations is more ambitious than the direct approaches which have been developed for steady, 1-D upwind discretizations (see e.g. Refs. 3,7 and 10); multi-D upwinding inherently leads to a greater sensitivity to noise and hence less robustness. Though Sidilkover does not show numerical results for real flow equations (such as e.g. the Euler equations), but confines himself to rather simple model equations, the numerical results presented in Ref. 19 are promising from a viewpoint of both accuracy and efficiency. They show that it is worthwhile to further investigate direct solution methods for multi-D upwind discretizations.

### 1.4 Present approach

In the present paper, we do not confine ourselves to a model equation. For the steady Euler equations, in a cell-centered finite volume context, we present and apply here two multi-D upwind schemes with some optimal balance between multi-D accuracy and efficiency. The steady equations are solved directly (so not through an unsteady form). For good efficiency, we rely on nonlinear multigrid (multigrid-Newton) iteration in the standard way (Ref. 4). As soon as we experience that local coarse-to-fine grid corrections are transferred which inhibit convergence, instead of standard nonlinear multigrid, we apply an improved nonlinear multigrid technique.

As the smoothing technique in the multigrid iteration, point Gauss-Seidel relaxation is applied, using the exact derivative matrices (exact Newton). The latter requires the cell face fluxes to be continuously differentiable. If the smoothing technique inhibits good convergence, we do not try to improve its smoothing properties, but - instead - we rely on defect correction iteration as the most outer iteration, just as in Refs. 5,11 and 12.

The multi-D upwind schemes to be considered here are very simple schemes. They use neither decoupling of the Euler equations (as in Refs. 8 and 18), nor rotated fluxes (as in Refs. 2 and 15). The schemes are based on *rotated left and right cell face states solely.* Per cell face, just as with grid-aligned 1-D upwind schemes, only a single numerical flux is computed: the one normal to the cell face. The only difference between grid-aligned 1-D upwind schemes and the present multi-D upwind schemes is that whereas in the first schemes the left and right cell face states are computed from a *solution-independent, 1-D* subset of the local multi-D solution, in the present multi-D upwind schemes, these states are computed from a *solution-dependent, multi-D* subset. The numerical flux function to be applied should allow a good resolution of both oblique shock waves and oblique contact discontinuities, which makes flux difference splitting schemes to be preferred above flux splitting schemes. Given the good experience with Osher's scheme (Ref. 16) in combination with nonlinear multigrid (Ref. 7), we apply this flux difference splitting scheme. The two multi-D upwind schemes to be presented are first analyzed on the basis of a model equation, discretized on a square, cell-centered finite volume grid.

## 2 Two multi-D upwind schemes for a model equation

The analysis is performed for the linear, scalar, 2-D model equation

$$\cos\theta\frac{\partial u}{\partial x}+\sin\theta\frac{\partial u}{\partial y}=0,\quad 0\le\theta\le\frac{\pi}{2}, \tag{2.1a}$$

with $\theta$ the angle between the characteristic direction and the $x$-axis (Fig. 2.1a). For ease of notation we introduce

$$\begin{pmatrix} a \\ b \end{pmatrix}\equiv\begin{pmatrix} \cos\theta \\ \sin\theta \end{pmatrix}. \tag{2.1b}$$

Discretization of the model equation on a square, cell-centered finite volume grid yields

$$a(u_{i+\frac{1}{2},j}-u_{i-\frac{1}{2},j})+b(u_{i,j+\frac{1}{2}}-u_{i,j-\frac{1}{2}})=0, \tag{2.2}$$

where the half-integer indices refer to the cell faces between the (full-integer indexed) cell centers (Fig. 2.1b).
With the standard, first-order, grid-aligned 1-D upwind scheme, given the positive sign of $a$ and $b$, for the cell face states one takes

$$\begin{pmatrix} u_{i+\frac{1}{2},j} \\ u_{i,j+\frac{1}{2}} \end{pmatrix}=\begin{pmatrix} u_{i,j} \\ u_{i,j} \end{pmatrix} \tag{2.3}$$

Similar choices are made for $u_{i-\frac{1}{2},j}$ and $u_{i,j-\frac{1}{2}}$. Substituting these cell face states into (2.2), applying truncated Taylor series expansions and transforming to characteristic coordinates, one derives the modified equation

$$\frac{\partial u}{\partial s}-\frac{h}{2}\left[(a^3+b^3)\frac{\partial^2 u}{\partial s^2}-2ab(a-b)\frac{\partial^2 u}{\partial s\partial n}+ab(a+b)\frac{\partial^2 u}{\partial n^2}\right]=O(h^2). \tag{2.4}$$

For convenience we introduce the notations $\mu_{ss},\mu_{sn}$ and $\mu_{nn}$ for the coefficients of $\frac{\partial^2 u}{\partial s^2}$, $\frac{\partial^2 u}{\partial s\partial n}$ and $\frac{\partial^2 u}{\partial n^2}$, respectively. For the specific model equation considered here, the error term $\mu_{nn}\frac{\partial^2 u}{\partial n^2}$ in (2.4) is most detrimental to accuracy. (The other two error terms just vanish for the model equation; $\frac{\partial u}{\partial s}=0$.) Hence, a higher-order accurate discretization can be constructed by only making $\mu_{nn}$ vanish. For the same model equation, compact multi-D upwind discretizations with only $\mu_{nn}=0$, have been investigated already in Ref. 19. However, no published results of that kind are available for the full Euler equations. In the present paper, we prefer compact multi-D upwind schemes with both $\mu_{sn}=0$ and $\mu_{nn}=0$; discretizations which guarantee a low crosswind diffusion for $\frac{\partial u}{\partial s}=r(s,n)$, with $r(s,n)$ arbitrary, instead of $r(s,n)=0$ only. In other words, we prefer discretizations which are more general by guaranteeing a certain accuracy for a specific model *operator* instead of for only a specific model *equation*. Further, we do make the extension from the linear scalar model operator to the Euler operator.

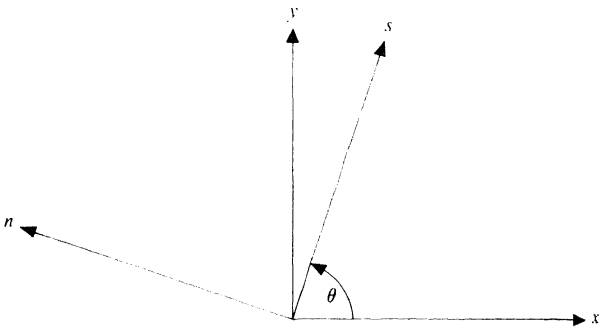


a. Angle characteristic direction and characteristic coordinates.

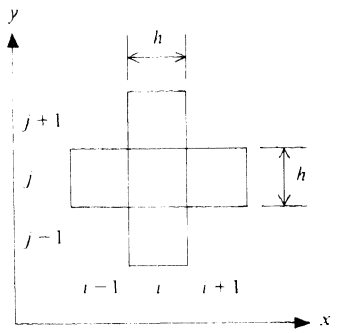


b. Square finite volume $i,j$ with four neighbors.

Fig. 2.1. Geometric situation.

**Definition 2.1**
Consider the general modified equation

$$\frac{\partial u}{\partial s}-\frac{h}{2}\left[\mu_{ss}\frac{\partial^2 u}{\partial s^2}+\mu_{sn}\frac{\partial^2 u}{\partial s\partial n}+\mu_{nn}\frac{\partial^2 u}{\partial n^2}\right]=O(h^2). \tag{2.5}$$

In this paper, $(\mu_{sn},\mu_{nn})^T$ is called the *crosswind diffusion*, and schemes for which $(\mu_{sn},\mu_{nn})^T=0$ are called *zero-crosswind diffusion schemes.*

From (2.4) it appears that for the grid-aligned scheme (2.3), zero-crosswind diffusion occurs only in case of $\theta=0$ or $\theta=\frac{\pi}{2}$, i.e. in case of grid-alignment of the characteristic direction. As opposed to these poor accuracy properties, the stability properties of scheme (2.3) are known to be good; the scheme does not allow unstable, oscillatory solutions. This results from the fact that the positive coefficients rule (Ref. 17) is satisfied, which clearly appears from its stencil

$$\begin{bmatrix} \cdot & \cdot & \cdot \\ -a & a+b & \cdot \\ \cdot & -b & \cdot \end{bmatrix}. \tag{2.6}$$

**Definition 2.2**
Consider the general discrete equation

$$\alpha_{i,j}u_{i,j}=\sum_{m=1}^{M}\sum_{n=1}^{N}\alpha_{i\pm m,j\pm n}u_{i\pm m,j\pm n},\quad M\ge 1,N\ge 1. \tag{2.7}$$

In this paper, discrete equations satisfying the positive coefficients rule

$$\alpha_{i,j}\ge 0,\quad \alpha_{i\pm m,j\pm n}\ge 0,\quad \forall\, m,n, \tag{2.8}$$

are called *positive.*

Concerning now multi-D upwind schemes, we would like to have schemes which satisfy all following five properties: (i) zero-crosswind diffusion, (ii) positivity, (iii) compactness, (iv) good smoothing of point Gauss-Seidel relaxation, and (v) continuous differentiability. The property of zero-crosswind diffusion is meant to lead to an accurate resolution of oblique layers. Positivity is strived for to avoid instabilities (without invoking a limiter). Compactness is to assure consistent boundary condition treatments. Good smoothing of point Gauss-Seidel relaxation should assure a fruitful application of multigrid, and continuous differentiability finally is required because of the intended application of Newton iteration inside the point relaxation.

### 2.1 A continuously differentiable scheme

For the $\theta$-range $0 \leq \theta \leq \frac{\pi}{2}$, multi-D upwind schemes which are most compact have as stencil

$$\begin{bmatrix} \cdot & \cdot & \cdot \\ -\alpha_{i-1,j} & \alpha_{i,j} & \cdot \\ -\alpha_{i-1,j-1} & -\alpha_{i,j-1} & \cdot \end{bmatrix}. \tag{2.9}$$

In an attempt (Ref. 6) to derive such a 4-point compact upwind scheme, which satisfies the foregoing five properties, we found the following limiting theorems:

**Theorem 2.1**
*No 4-point compact upwind scheme exists for which both* $\mu_{sn} = 0$ *and* $\mu_{nn} = 0$.

**Theorem 2.2**
*No 4-point compact upwind scheme exists which is positive and for which* $\mu_{nn} = 0$.

However, in Ref. 6 we did find a 4-point compact scheme, by only requiring $\mu_{sn} = 0$ to hold in combination with the property of positivity. The scheme reads

$$\begin{pmatrix} u_{i+\frac{1}{2},j} \\ u_{i,j+\frac{1}{2}} \end{pmatrix} = \begin{pmatrix} \frac{a+\frac{1}{2}b}{a+b} u_{i,j} + \frac{\frac{1}{2}b}{a+b} u_{i,j-1} \\ \frac{b+\frac{1}{2}a}{a+b} u_{i,j} + \frac{\frac{1}{2}a}{a+b} u_{i-1,j} \end{pmatrix}, \tag{2.10}$$

which gives the stencil

$$\begin{bmatrix} \cdot & \cdot & \cdot \\ \frac{-a^2}{a+b} & \frac{1+ab}{a+b} & \cdot \\ \frac{-ab}{a+b} & \frac{-b^2}{a+b} & \cdot \end{bmatrix}, \tag{2.11}$$

and the modified equation

$$\frac{\partial u}{\partial s} - \frac{h}{2}\left[\frac{1+ab}{a+b}\frac{\partial^2 u}{\partial s^2} + \frac{ab}{a+b}\frac{\partial^2 u}{\partial n^2}\right] = O(h^2). \tag{2.12}$$

### 2.2 A zero-crosswind diffusion scheme

To remove all crosswind diffusion, wider stencils must be considered. Following the modified equation approach, in Ref. 6 we have derived a 6-point compact scheme with zero-crosswind diffusion over the complete range of $\theta$ considered; $0 \leq \theta \leq \frac{\pi}{2}$. Summarizing, we have derived as expressions for the cell face states, for the subranges $0 \leq \theta \leq \frac{\pi}{4}$ and $\frac{\pi}{4} \leq \theta \leq \frac{\pi}{2}$, respectively:

$$\begin{pmatrix} u_{i+\frac{1}{2},j} \\ u_{i,j+\frac{1}{2}} \end{pmatrix} = \begin{pmatrix} u_{i,j} \\ \frac{1}{2}(1+\frac{b}{a})u_{i-1,j} + \frac{1}{2}(1-\frac{b}{a})u_{i-1,j+1} \end{pmatrix}, \tag{2.13a}$$

$$\begin{pmatrix} u_{i+\frac{1}{2},j} \\ u_{i,j+\frac{1}{2}} \end{pmatrix} = \begin{pmatrix} \frac{1}{2}(1+\frac{a}{b})u_{i,j-1} + \frac{1}{2}(1-\frac{a}{b})u_{i+1,j-1} \\ u_{i,j} \end{pmatrix}. \tag{2.13b}$$

The corresponding stencils are:

$$\begin{bmatrix} \frac{1}{2}b(1-\frac{b}{a}) & \cdot & \cdot \\ b(\frac{b}{a}-\frac{a}{b}) & a & \cdot \\ -\frac{1}{2}b(1+\frac{b}{a}) & \cdot & \cdot \end{bmatrix}, \tag{2.14a}$$

$$\begin{bmatrix} \cdot & \cdot & \cdot \\ \cdot & b & \cdot \\ -\frac{1}{2}a(1+\frac{a}{b}) & a(\frac{a}{b}-\frac{b}{a}) & \frac{1}{2}a(1-\frac{a}{b}) \end{bmatrix}, \tag{2.14b}$$

and the corresponding modified equations:

$$\frac{\partial u}{\partial s} - \frac{h}{2}\frac{1}{a}\frac{\partial^2 u}{\partial s^2} = O(h^2), \tag{2.15a}$$

$$\frac{\partial u}{\partial s} - \frac{h}{2}\frac{1}{b}\frac{\partial^2 u}{\partial s^2} = O(h^2). \tag{2.15b}$$

## 3 The two multi-D upwind schemes for the Euler equations

An important difference between model equation (2.1a) and the Euler equations is that for the latter, $\theta$ is no longer a constant and not even a scalar. Yet, for the Euler equations, in both present multi-D upwind schemes, per cell face we determine and use a single rotation angle only. Here, first the use of this angle is discussed by generalizing the two schemes from the foregoing section to the 2-D Euler equations.

The extension is straightforward. Because in the model equation the characteristic information was coming from the left, for the Eulerian numerical flux function, the components of the left cell face states are computed in the same way as the cell face states for the model equation. For the right cell face states, we simply take the point symmetric counterpart of the left states. In this way, in case of all characteristic information coming from the right (supersonic flow from the right), one also has the proper discretization.

### 3.1 The continuously differentiable scheme

For the left cell face states to be substituted into the Eulerian numerical flux function, continuously differentiable scheme (2.10) as derived for model equation (2.1), is applied as

$$\begin{pmatrix} q_{i+\frac{1}{2},j} \\ q_{i,j+\frac{1}{2}} \end{pmatrix}^l = \frac{1}{1+\tan\theta}\begin{pmatrix} (1+\frac{1}{2}\tan\theta)q_{i,j} + \frac{1}{2}\tan\theta q_{i,j-1} \\ (\frac{1}{2}+\tan\theta)q_{i,j} + \frac{1}{2}q_{i-1,j} \end{pmatrix}, \tag{3.1}$$

and for the right cell face states it is applied as

$$\begin{pmatrix} q_{i+\frac{1}{2},j} \\ q_{i,j+\frac{1}{2}} \end{pmatrix}^r = \frac{1}{1+\tan\theta}\begin{pmatrix} (1+\frac{1}{2}\tan\theta)q_{i+1,j} + \frac{1}{2}\tan\theta q_{i+1,j+1} \\ (\frac{1}{2}+\tan\theta)q_{i,j+1} + \frac{1}{2}q_{i+1,j+1} \end{pmatrix}. \tag{3.2}$$

### 3.2 The zero-crosswind diffusion scheme

Zero-crosswind diffusion scheme (2.13) as derived for model equation (2.1) is applied to the Euler equations as

$$\begin{pmatrix} q_{i+\frac{1}{2},j} \\ q_{i,j+\frac{1}{2}} \end{pmatrix}^l = \begin{pmatrix} q_{i,j} \\ \frac{1}{2}(1+\tan\theta)q_{i-1,j} + \frac{1}{2}(1-\tan\theta)q_{i-1,j+1} \end{pmatrix}, \tag{3.3a}$$

$$\begin{pmatrix} q_{i+\frac{1}{2},j} \\ q_{i,j+\frac{1}{2}} \end{pmatrix}^l = \begin{pmatrix} \frac{1}{2}(1+\frac{1}{\tan\theta})q_{i,j-1} + \frac{1}{2}(1-\frac{1}{\tan\theta})q_{i+1,j-1} \\ q_{i,j} \end{pmatrix}, \tag{3.3b}$$

and

$$\begin{pmatrix} q_{i+\frac{1}{2},j} \\ q_{i,j+\frac{1}{2}} \end{pmatrix}^r = \begin{pmatrix} q_{i+1,j} \\ \frac{1}{2}(1+\tan\theta)q_{i+1,j+1} + \frac{1}{2}(1-\tan\theta)q_{i+1,j} \end{pmatrix}, \tag{3.4a}$$

$$\begin{pmatrix} q_{i+\frac{1}{2},j} \\ q_{i,j+\frac{1}{2}} \end{pmatrix}^r = \begin{pmatrix} \frac{1}{2}(1+\frac{1}{\tan\theta})q_{i+1,j+1} + \frac{1}{2}(1-\frac{1}{\tan\theta})q_{i,j+1} \\ q_{i,j+1} \end{pmatrix}. \tag{3.4b}$$

## 4 Rotation angles for the Euler equations

Per cell face we select a single rotation angle $\theta$ from the local, multi-D solution. For this, in Ref. 6 a technique is derived which looks at all cell faces at either the local flow angle only, or a local shock wave angle only. The technique considers a wave path in state space: the one of the P-variant of Osher's scheme (Ref. 7). Here we just summarize the practical outcome of the derivation given in Ref. 6. Taking for the left and right wave path states $q_0$ and $q_1$ (at all cell faces $i+\frac{1}{2}, j$ and $i, j+\frac{1}{2}$), e.g.

$$\begin{pmatrix} q_{i+\frac{1}{2},j} \\ q_{i,j+\frac{1}{2}} \end{pmatrix}_0 = \begin{pmatrix} q_{i,j} \\ q_{i,j} \end{pmatrix}, \tag{4.1a}$$

$$\begin{pmatrix} q_{i+\frac{1}{2},j} \\ q_{i,j+\frac{1}{2}} \end{pmatrix}_1 = \begin{pmatrix} q_{i+1,j} \\ q_{i,j+1} \end{pmatrix}, \tag{4.1b}$$

we found that the orientation of a contact discontinuity follows from the (novel) relation

$$\tan\theta = \frac{\alpha v_0 + v_1}{\alpha u_0 + u_1}, \tag{4.2a}$$

with

$$\alpha \equiv \sqrt{\frac{\rho_0}{\rho_1}\left(\frac{p_1}{p_0}\right)^{\frac{1}{\gamma}}} \tag{4.2b}$$

In here, $u, v, \rho, p$ and $\gamma$ denote successively: the velocity components in $x$- and $y$-direction, density, pressure and the specific heat ratio.
Further, for the orientation of a shock wave, we found the (known) relation

$$\tan\theta = \frac{u_0 - u_1}{v_0 - v_1}. \tag{4.3}$$

# 5 Multigrid and Defect Correction

For the discretized equations corresponding with (3.1)-(3.2), in Ref. 6 it is shown that these allow an efficient smoothing by point Gauss-Seidel relaxation. Due to their non-positivity, no such efficient smoother exists for the discretized equations corresponding with scheme (3.3)-(3.4). To solve the latter equations, we rely on defect correction iteration with continuously differentiable scheme as the 'working horse' scheme in the inner multigrid iteration.

Concerning the multigrid iteration, for hypersonic flow computations we often experience that coarse-to-fine grid corrections are transferred which lead to divergence. In Ref. 13 - as remedies to this - we derived: (i) a local damping technique for the defect and hence - implicitly - a local damping technique for the correction, and (ii) a global upwind prolongation technique for the correction. Here the practical outcome of this analysis is summarized.

## 5.1 Local defect damping

The advantage of *defect* damping instead of *correction* damping is that it is more a-priori and hence safer. (Correction damping may more easy be too late.) Further, the advantage of *local* damping instead of *global* damping is that it is better dosed. (Global damping may also reduce the *positive* effects of a coarse grid correction.) To summarize the local defect damping, let

$$N_l(q_l) = r_l \tag{5.1}$$

denote the nonlinear system of equations that one wants to solve at grid level $l$. Then the corresponding $(n+1)$st coarse grid problem ($n = 0, 1, \ldots, N$) to be solved, reads

$$N_{l-1}(q_{l-1}^{n+1}) = N_{l-1}(q_{l-1}^{n}) - S_{l-1} I_l^{l-1}(N_l(q_l^{n+\frac{1}{3}}) - r_l), \tag{5.2}$$

with $S_{l-1}$ denoting the operator for the defect damping, with $q_l^{n+\frac{1}{3}}$ denoting the fine grid iterate as obtained after the (fine grid) pre-relaxation, and with $q_{l-1}^{n}$ and $q_{l-1}^{n+1}$ denoting the coarse grid iterates before the (coarse grid) pre-relaxation and after the (coarse grid) post-relaxation, respectively. In Ref. 13, for optimal two-grid convergence, from (5.1)-(5.2) we have derived as local damping factor for the defect in the $(i,j)$th finite volume at level $l-1$:

$$(S_{l-1}^{n+1})_{i,j} = \min\left(1, \frac{\|(N_{l-1}')_{i,j}\|}{\|(N_l')_{i,j}\|}\right), \tag{5.3a}$$

with

$$\|(N_l')_{i,j}\| \equiv \max\Big(\|(N_l')_{2i-1,2j-1}\|, \|(N_l')_{2i,2j}\|, \|(N_l')_{2i-1,2j}\|, \|(N_l')_{2i,2j-1}\|\Big), \tag{5.3b}$$

and with $N_{l-1}' \equiv \mathrm{d}N_{l-1}(q_{l-1}^{n})/\mathrm{d}q_{l-1}$, $N_l' \equiv \mathrm{d}N_l(q_l^{n+\frac{1}{3}})/\mathrm{d}q_l$, and $\|\cdot\|$ some user-defined matrix norm. At convergence of the solution, the defect damping will also have converged. However, notice that the damping will not necessarily have vanished at convergence.

## 5.2 Global upwind prolongation

Writing the standard, piecewise constant correction prolongation as

$$\begin{pmatrix} (q_l^{\mathrm{new}})_{2i-1,2j-1} \\ (q_l^{\mathrm{new}})_{2i-1,2j} \\ (q_l^{\mathrm{new}})_{2i,2j-1} \\ (q_l^{\mathrm{new}})_{2i,2j} \end{pmatrix} = \begin{pmatrix} (q_l^{\mathrm{old}})_{2i-1,2j-1} \\ (q_l^{\mathrm{old}})_{2i-1,2j} \\ (q_l^{\mathrm{old}})_{2i,2j-1} \\ (q_l^{\mathrm{old}})_{2i,2j} \end{pmatrix} + (\Delta q_{l-1})_{i,j} \begin{pmatrix} 1 \\ 1 \\ 1 \\ 1 \end{pmatrix}, \tag{5.4a}$$

with

$$(\Delta q_{l-1})_{i,j} \equiv (q_{l-1}^{\mathrm{new}})_{i,j} - (q_{l-1}^{\mathrm{old}})_{i,j}, \tag{5.4b}$$

the upwind correction prolongation reads

$$\begin{pmatrix} (q_l^{\mathrm{new}})_{2i-1,2j-1} \\ (q_l^{\mathrm{new}})_{2i-1,2j} \\ (q_l^{\mathrm{new}})_{2i,2j-1} \\ (q_l^{\mathrm{new}})_{2i,2j} \end{pmatrix} = \begin{pmatrix} (q_l^{\mathrm{old}})_{2i-1,2j-1} \\ (q_l^{\mathrm{old}})_{2i-1,2j} \\ (q_l^{\mathrm{old}})_{2i,2j-1} \\ (q_l^{\mathrm{old}})_{2i,2j} \end{pmatrix} + \frac{1}{2}\begin{pmatrix} (\Delta q_{l-1})_{i-\frac{1}{2},j} \\ (\Delta q_{l-1})_{i-\frac{1}{2},j} \\ (\Delta q_{l-1})_{i+\frac{1}{2},j} \\ (\Delta q_{l-1})_{i+\frac{1}{2},j} \end{pmatrix} + \frac{1}{2}\begin{pmatrix} (\Delta q_{l-1})_{i,j-\frac{1}{2}} \\ (\Delta q_{l-1})_{i,j+\frac{1}{2}} \\ (\Delta q_{l-1})_{i,j-\frac{1}{2}} \\ (\Delta q_{l-1})_{i,j+\frac{1}{2}} \end{pmatrix}, \tag{5.5a}$$

so with the four fine grid cell center corrections defined as *central* averages of the coarse grid cell face corrections. The coarse grid cell face corrections now, are defined by

$$\begin{pmatrix} (\Delta q_{l-1})_{i-\frac{1}{2},j} \\ (\Delta q_{l-1})_{i+\frac{1}{2},j} \\ (\Delta q_{l-1})_{i,j-\frac{1}{2}} \\ (\Delta q_{l-1})_{i,j+\frac{1}{2}} \end{pmatrix} \equiv \begin{pmatrix} (q_{l-1}^{\mathrm{new}})_{i-\frac{1}{2},j} \\ (q_{l-1}^{\mathrm{new}})_{i+\frac{1}{2},j} \\ (q_{l-1}^{\mathrm{new}})_{i,j-\frac{1}{2}} \\ (q_{l-1}^{\mathrm{new}})_{i,j+\frac{1}{2}} \end{pmatrix} - \begin{pmatrix} (q_{l-1}^{\mathrm{old}})_{i-\frac{1}{2},j} \\ (q_{l-1}^{\mathrm{old}})_{i+\frac{1}{2},j} \\ (q_{l-1}^{\mathrm{old}})_{i,j-\frac{1}{2}} \\ (q_{l-1}^{\mathrm{old}})_{i,j+\frac{1}{2}} \end{pmatrix}, \tag{5.5b}$$

where the coarse grid cell face states are computed in an *upwind* manner. We remark that when applying the P-variant of Osher's scheme, in most cases, upwind computation of the cell face states is trivial. (For details we refer to Ref. 13.)

# 6 Numerical results

For the steady, 2-D Euler equations and a perfect gas with $\gamma = 1.4$, numerical experiments are performed for: (i) some supersonic, unit square flows with either oblique contact discontinuity or oblique shock wave, and for (ii) a hypersonic blunt body flow. The supersonic flows are considered for illustrating the properties of the two multi-D upwind schemes, the hypersonic problem for illustrating the benefits of the multigrid improvements.

## 6.1 Supersonic, unit square flows

First, flows with contact discontinuity are considered for the flow angles $\theta = 0.1\pi, 0.2\pi, 0.3\pi$ and $0.4\pi$ (Fig. 6.1a). Next, flows with shock wave are considered for the shock wave angles $\theta = \frac{\pi}{4}$ and $\theta = \frac{\pi}{8}$ (Fig. 6.1b). All these flows are computed on a uniform $32 \times 32$-grid. In all cases - for simplicity - at each of the four boundaries, the exact solution is imposed (overspecification). Further, in all cases, the problem is solved by a standard nonlinear multigrid method (FAS); with a $2 \times 2$-grid as the coarsest grid, with V-cycles, and with a single pre- and post-relaxation sweep per level. We remark that with scheme (3.1)-(3.2) to be locally linearized in the inner multigrid iteration, one has $4 \times 4$ derivative matrices containing contributions which originate from the solution-dependent rotation angle. In all cases we take as the initial solution: the solution with $q = q^L$ (the exact $q^L$'s from Figs. 6.1a and 6.1b) uniformly constant over the complete domain.

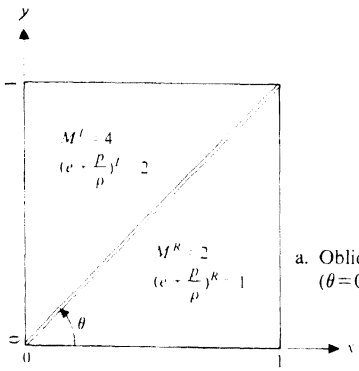


a. Oblique contact discontinuity ($\theta = 0.1\pi, 0.2\pi, 0.3\pi, 0.4\pi$, $p = 1$).

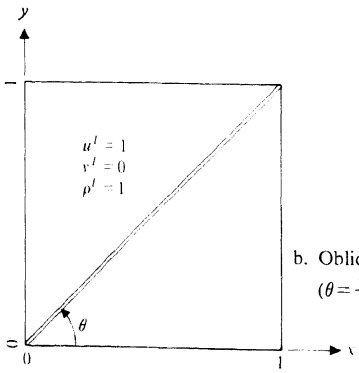


b. Oblique shock wave ($\theta = \frac{\pi}{4}, M^l = 2$ and $\theta = \frac{\pi}{8}, M^l = 4$).

Fig. 6.1. Supersonic, unit square flows.

### 6.1.1 Flows with contact discontinuity

First, in Fig. 6.2, reference results are given for the present four test cases; results obtained by the first-order, grid-aligned 1-D upwind scheme. In Fig. 6.2a, we plotted on top of each other: the enthalpy $(e + \frac{p}{\rho})$ distributions for $\theta = 0.1\pi, 0.2\pi, 0.3\pi$ and $0.4\pi$. The iso-enthalpy values considered in these and all following enthalpy distributions are: $1.1, 1.2, 1.3, \ldots, 1.9$. Because of the severe smearing of the first-order, grid-aligned 1-D upwind scheme, hardly any distinction can be made between the four solutions. (Notice that the layers along $x = 1$ and $y = 1$ in Fig. 6.2a, and also in the following enthalpy graphs, are only due to the overspecification.) The convergence histories corresponding with the first-order, grid-aligned 1-D upwind scheme, are given in Fig. 6.2b.

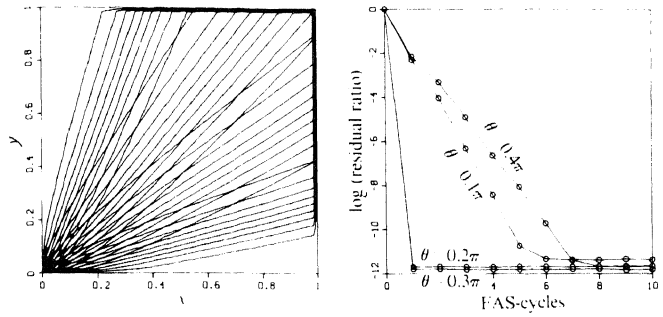


a. Enthalpy distributions. b. Multigrid convergence histories.

Fig. 6.2. Results first-order, grid-aligned 1-D upwind scheme, flows with contact discontinuity.

In Fig. 6.3, results are given as obtained by multi-D scheme (3.1)-(3.2), with as the rotation angle: the local flow angle according to (4.2). Though more accurate than the grid-aligned reference distributions in Fig. 6.2a, the present enthalpy distributions (Fig. 6.3a) are still insufficiently accurate. Though not as very fast as the reference convergence in Fig. 6.2b, the present scheme's multigrid convergence (Fig. 6.3b) is still very good.

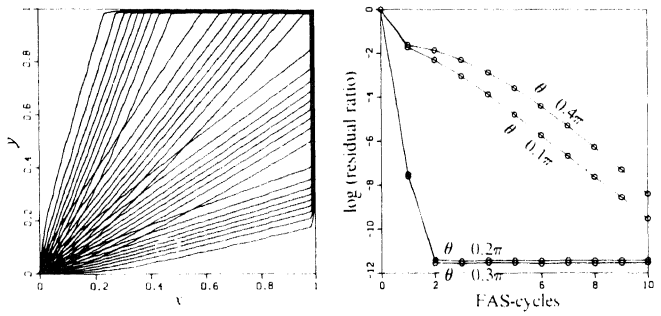


a. Enthalpy distributions. b. Multigrid convergence histories.

Fig. 6.3. Results continuously differentiable scheme (3.1)-(3.2), flows with contact discontinuity.

In Fig. 6.4 we give the enthalpy distributions for zero-crosswind diffusion scheme (3.3)-(3.4), as obtained after 10 defect correction cycles (with a single nonlinear multigrid cycle per defect correction cycle), and with also (4.2) for the rotation angle considered at each cell face. All enthalpy distributions appear to be almost free of crosswind diffusion. Although in principle the non-positivity of the scheme allows solutions with spurious oscillations, the distributions in Fig. 6.4 are still monotone.

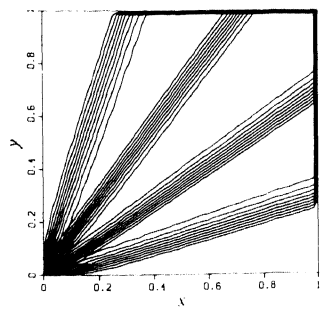


Fig. 6.4. Enthalpy distributions zero-crosswind diffusion scheme (3.3)-(3.4), flows with contact discontinuity.

### 6.1.2 Flows with shock wave

Reference results obtained by the first-order, grid-aligned 1-D upwind scheme - Mach number distributions - are given in Fig. 6.5a. Here solutions are also plotted on top of each other. The iso-Mach number values shown are: (i) $1.50, 1.55, 1.60, \ldots, 1.95$ for the case with $\theta = \frac{\pi}{4}, M^L = 2$, and (ii) $3.30, 3.35, 3.40, \ldots, 3.95$ for the case with $\theta = \frac{\pi}{8}, M^L = 4$. Similar to the flows with contact discontinuity, the layers along $x = 1$ and $y = 1$ are caused by the overspecification.

In Fig. 6.5b we give the Mach number distributions as obtained after two defect correction cycles with zero-crosswind diffusion scheme (3.3)-(3.4). The rotation angle considered here is the shock wave angle according to (4.3). After two defect correction cycles, the solution seems to be free of crosswind diffusion, but for $\theta = \frac{\pi}{4}$ it has become non-monotone. Construction of a compact multi-D limiter might be useful.

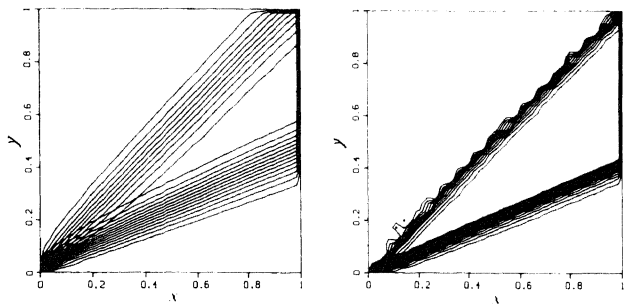


a. First-order, grid-aligned 1-D upwind scheme. b. Zero-crosswind diffusion scheme (3.3)-(3.4).

Fig. 6.5. Mach number distributions, flows with shock wave.

## 6.2 Hypersonic reentry flow

In all foregoing supersonic computations, the multigrid improvements from section 5 did not need to be invoked. Standard nonlinear multigrid worked satisfactory in all cases. Here three convergence behaviors are presented, as obtained through three different solution methods, for a hypersonic reentry flow: a flow around a double ellipse at $M_\infty = 8.15$, $\alpha = 30^\circ$, with as (finest) grid considered: the $128 \times 64$ C-type grid given in Fig. 6.6.

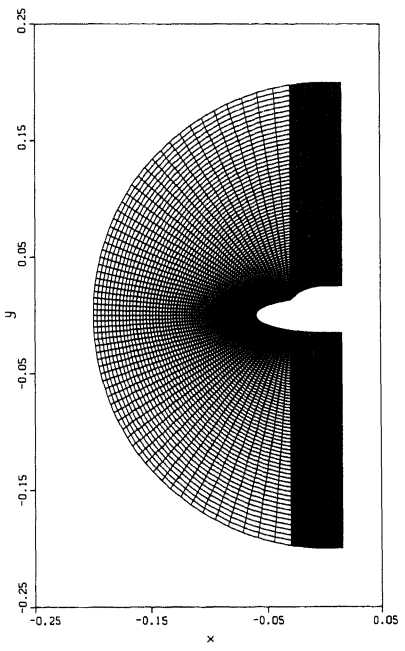


Fig. 6.6. $128 \times 64$-grid double ellipse.

All three solution methods are applied to the first-order, grid-aligned 1-D upwind discretized equations. The three methods considered are: (i) single-grid, (ii) standard nonlinear multigrid, and (iii) improved nonlinear multigrid. In both multigrid methods, the coarsest grid considered is a $4 \times 2$-grid. The convergence behaviors are given in Fig. 6.7a. Given the very low convergence rate of the single-grid computation, and given the absolute failure of the standard nonlinear multigrid method, the new multigrid constituents do not just appear to be a nice luxury, but a really useful tool. To give an indication of the defect damping, in Fig. 6.7b the converged damping factor distribution is shown. We remark that the damping is mainly restricted to the bow shock region.

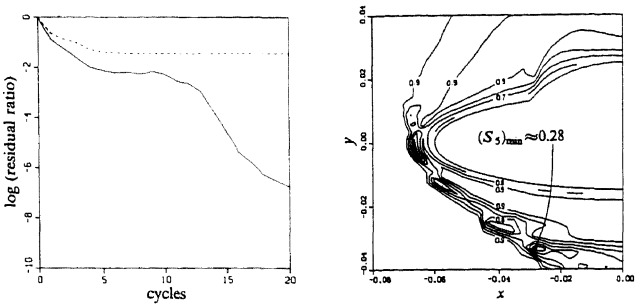


a. Convergence histories:
------ : single-grid,
..... : standard nonlinear multigrid,
—— : improved nonlinear multigrid.

b. Damping factor distribution.

Fig. 6.7. Results hypersonic reentry flow.

## 7 Conclusions

Multi-D upwinding through a 1-D Riemann solver with a local, solution-dependent rotation of the left and right Riemann states, allows to keep the number of flux computations per cell face equal to one only. Good efficiency is further guaranteed through nonlinear multigrid iteration and defect correction iteration. The accuracy and efficiency of the multi-D results are promising. One important result is that for flows with contact discontinuities, the performance of nonlinear multigrid with point Gauss-Seidel relaxation is good when one applies the positive, continuously differentiable scheme. Another important result is that, also for flows with contact discontinuities, the solutions obtained by the zero-crosswind diffusion scheme, appear to be nearly free of any crosswind diffusion. Moreover, their computation by means of defect correction iteration (with the positive, continuously differentiable scheme as the approximate scheme) is efficient. The zero-crosswind diffusion scheme seems to be well-suited for an accurate and efficient computation of e.g. vortex flows.

For the hypersonic test case considered, it appears that the combination of (local) damping of the defect and (global) upwind prolongation of the correction, is a satisfactory remedy against divergence of standard nonlinear multigrid.

All numerical techniques presented in this paper do not require any tuning of parameters. Further, the techniques can be carried over to 3-D, and - as far as not yet shown - they can be extended to non-Cartesian grids.

## 8 References


1. Catalano, L.A. and Deconinck, H. (1991), Two-dimensional optimization of smoothing properties of multi-stage schemes applied to hyperbolic equations, *Proceedings of the Third European Conference on Multigrid Methods*, Bonn, Germany.
2. Davis, S.F. (1984), A rotationally biased upwind difference scheme for the Euler equations, *J. Comput. Phys.* **56**, 65-92.
3. Dick, E. (1989), A multigrid flux-difference splitting method for steady Euler equations, *Proceedings of the Fourth Copper Mountain Conference on Multigrid Methods*, Copper Mountain, USA (SIAM, Philadelphia).
4. Hackbusch, W. (1985), *Multi-Grid Methods and Applications* (Springer, Berlin).
5. Hemker, P.W. (1986), Defect correction and higher order schemes for the multi grid solution of the steady Euler equations, *Proceedings of the Second European Conference on Multigrid Methods*, Cologne, Germany (Springer, Berlin).
6. Hemker, P.W. and Koren, B. (1991), Efficient multi-dimensional upwinding for the steady Euler equations, *Report NM-R9107* (CWI, Amsterdam).
7. Hemker, P.W. and Spekreijse, S.P. (1986), Multiple grid and Osher's scheme for the efficient solution of the steady Euler equations, *Appl. Numer. Math.* **2**, 475-493.
8. Hirsch, Ch., Lacor, C. and Deconinck, H. (1987), Convection algorithms based on a diagonalization procedure for the multidimensional Euler equations, *AIAA Paper 87-1163.*
9. Hirsch, Ch. and Lacor, C. (1989), Upwind algorithms based on a diagonalization of the multidimensional Euler equations, *AIAA Paper 89-1958.*
10. Jespersen, D.C. (1983), Design and implementation of a multigrid code for the Euler equations, *Appl. Math. Comput.* **13**, 357-374.
11. Koren, B. (1988), Defect correction and multigrid for an efficient and accurate computation of airfoil flows, *J. Comput. Phys.* **77**, 183-206.
12. Koren, B. (1990), Multigrid and defect correction for the steady Navier-Stokes equations, *J. Comput. Phys.* **87**, 25-46.
13. Koren, B. and Hemker, P.W. (1991), Damped, direction-dependent multigrid for hypersonic flow computations, *Appl. Numer. Math.* **7**, 309-328.
14. LeVeque, R.J. (1988), High resolution finite volume methods on arbitrary grids via wave propagation, *J. Comput. Phys.* **78**, 36-63.
15. Levy, D.W., Powell, K.G. and Van Leer, B. (1989), An implementation of a grid-independent upwind scheme for the Euler equations, *AIAA Paper 89-1931.*
16. Osher, S. and Solomon, F. (1982), Upwind difference schemes for hyperbolic systems of conservation laws, *Math. Comput.* **38**, 339-374.
17. Patankar, S.V. (1980), *Numerical Heat Transfer and Fluid Flow* (Hemisphere, New York).
18. Roe, P.L. (1986), Discrete models for the numerical analysis of time-dependent multidimensional gas dynamics, *J. Comput. Phys.* **63**, 458-476.
19. Sidilkover, D. (1989), Numerical solution to steady-state problems with discontinuities, *doctoral thesis* (Weizmann Institute of Science, Rehovot).